nature sustainability

ARTICLES

https://doi.org/10.1038/s41893-021-00836-x

Check for updates

Coloured low-emissivity films for building envelopes for year-round energy savings

Yucan Peng[1,6], Lingling Fan[2,6], Weiliang Jin[2,6], Yusheng Ye[1], Zhuojun Huang[1], Shang Zhai[3], Xuan Luo[4], Yinxing Ma[1], Jing Tang[1], Jiawei Zhou[1], Louisa C. Greenburg[1], Arun Majumdar[3], Shanhui Fan[2] and Yi Cui[1,5]✉

Buildings are responsible for over 40% of total US energy use, of which about 40% is directly related to the operation of heating, ventilation and air-conditioning (HVAC) systems. Saving energy to heat and cool buildings would contribute substantially to sustainability. Here we propose a category of coloured low-emissivity films for building walls that constitute the main component of the building thermal envelope. We demonstrate high reflectance (~90%) in infrared wavelength range and selective reflectance in the visible light wavelength range for desired colours. These films can help minimize radiative heat exchange between the indoor and outdoor environments, thus saving energy for all-year cooling and heating while satisfying the required aesthetical effect. Simulations show that these films can help reduce heat gain and loss by up to 257.6 MJ per installation wall area annually. In the case of a typical midrise apartment building, the HVAC system can save up to 124.46 GJ (equal to 9.87% of the building's HVAC energy consumption). By rough estimation, a global CO_2 emission reduction of 1.14 billion metric tons annually could be achieved. Our work provides insights for innovative energy-saving building envelope materials that can help achieve global carbon neutrality and sustainability.

Buildings are important users of energy in present-day society, and energy-efficient buildings play an increasingly important role in sustainability[1]. More than 76% of total electricity and 40% of all energy in the United States are consumed to provide comfortable, well-lit and well-conditioned buildings[2], which results in a cost of more than $430 billion annually and substantial global greenhouse gas emission[3,4]. The heating, ventilation and air-conditioning (HVAC) systems of buildings contribute to about 40% of the building energy consumption, which is directly related to the heating and cooling demands of buildings[5]. This huge energy consumption is causing severe environmental and economic problems. It is therefore essential to develop innovations of science and technology to achieve improved energy efficiency of building HVAC with a reduced carbon footprint.

In addition to building insulation materials with low thermal conductivity such as expanded polystyrene, vacuum insulation panels and aerogels[6], engineering the radiative properties of building envelopes is emerging as a promising approach for building energy savings. For instance, near-infrared (NIR) reflective cooling coatings have been developed. These coatings reflect the invisible NIR light in the solar spectrum to decrease solar heating, but they show visible colours[7]. Additionally, passive daytime radiative cooling materials create a surface that has high solar reflectance and high emittance in the mid-infrared (MIR) transparent window of the atmosphere for saving cooling energy by rejecting solar heating and radiating heat to the cold sky[4,8–12]. These materials are suitable for unshaded building roofs to efficiently radiate heat to the outer space or sky, and the ideal installation locations should have long and warm summers to avoid a heating penalty in winters[13,14]. For building walls, unlike for roofs facing the sky, the MIR radiative heat exchange is more dominant with outdoor ambient surroundings than with the sky[15]. Such radiative heat exchange is more pronounced in urban areas, where buildings are concentrated. Traditional building materials usually show high thermal emissivity[16,17], leading to intense radiative heat exchange. In hot climates, the overheating caused by high radiation throughput from the hot environment and the sun results in increased cooling demand. Similarly, the excessive radiative heat loss from the building interior in cold climates leads to increased heating energy consumption. A design that minimizes radiative heat transfer through the building wall envelope will therefore be beneficial for both cooling and heating energy savings throughout the year[18].

Applying low-emissivity materials to the building envelope has been shown to be a promising strategy[19,20]. Metalized and metal films or foils (laminated with other materials)[21,22] and low-emissivity paints containing heat-reflective aluminium (Al) or silver dust as radiant barriers have been proposed to be installed with sufficient air layers, usually within the building envelopes[23]. These materials create more reflective surfaces for hollow bricks[24], roof attics[25] and exterior or interior wall surfaces[26–28]. However, regardless of their thermal performance, the state-of-the-art low-emissivity materials are commonly a metallized silver colour and suffer from severe aesthetical limitation, which tremendously hinders their extensive practical applications. It is important to develop materials that satisfy people's aesthetical demands while still achieving energy-efficient buildings.

Here we develop a category of coloured low-emissivity films for building wall thermal envelopes, providing a solution to year-round building heating and cooling energy savings. These coloured low-emissivity films aim to realize the thermal regulation and

[1]Department of Materials Science and Engineering, Stanford University, Stanford, CA, USA. [2]E. L. Ginzton Laboratory, Department of Electrical Engineering, Stanford University, Stanford, CA, USA. [3]Department of Mechanical Engineering, Stanford University, Stanford, CA, USA. [4]Building Technology and Urban Systems Division, Lawrence Berkeley National Laboratory, Berkeley, CA, USA. [5]Stanford Institute for Materials and Energy Sciences, SLAC National Accelerator Laboratory, Menlo Park, CA, USA. [6]These authors contributed equally: Yucan Peng, Lingling Fan, Weiliang Jin. ✉e-mail: yicui@stanford.edu

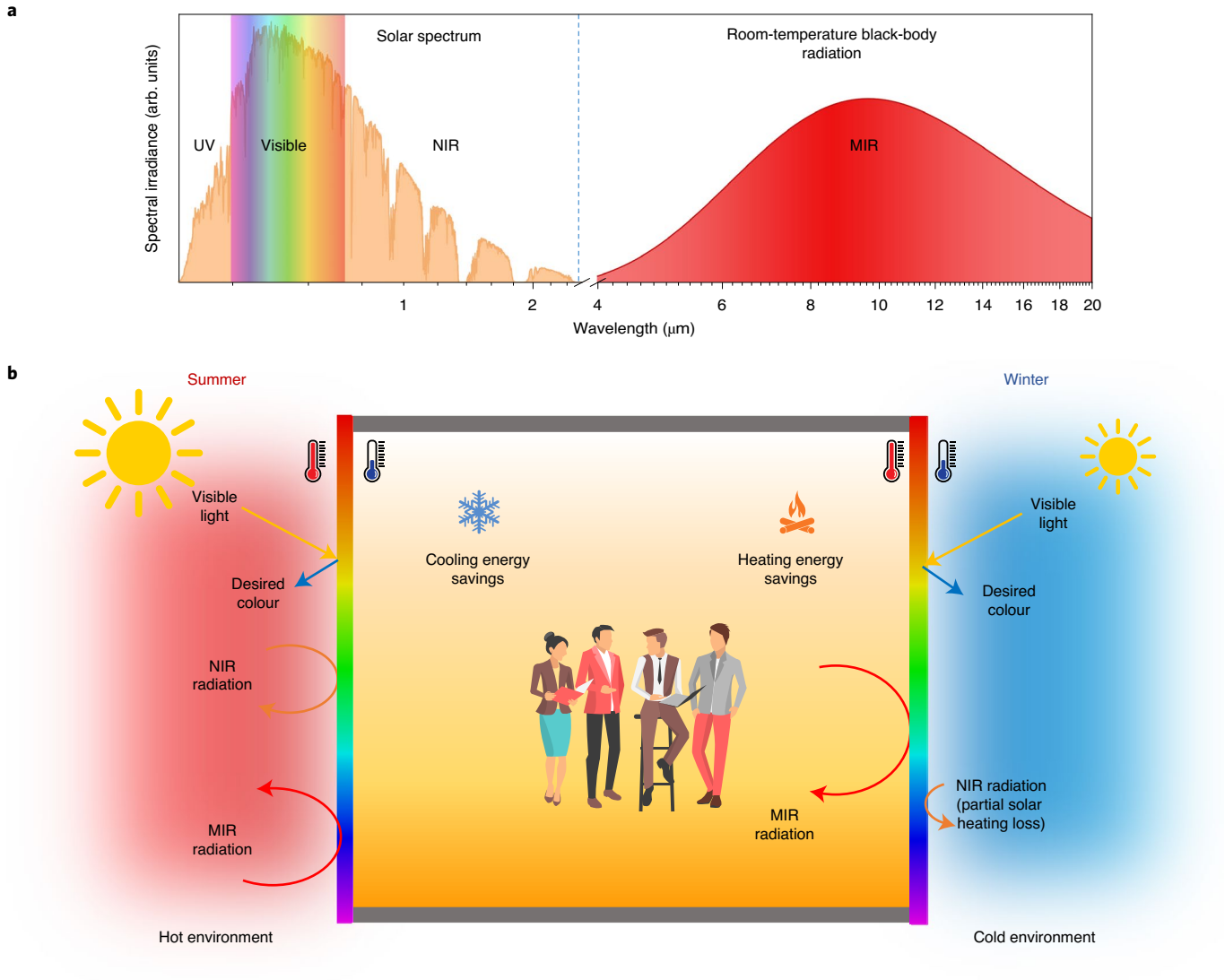

Fig. 1 | Concept illustration. a, Spectra of solar irradiation (plotted by AM 1.5G, global tilt) and room-temperature thermal radiation simulated using Planck's law at 300 K. UV, ultraviolet. **b**, These coloured low-emissivity films aim to realize the thermal regulation purpose and the aesthetical demand simultaneously. The optical properties of the coloured low-emissivity films are engineered to be spectrally selective. In the visible light wavelength range (400–700 nm), only light in the desired colour wavelength range is reflected to fulfil the aesthetical function. In the MIR wavelength range, the films are highly reflective to minimize radiative thermal exchange with hot and cold environments. In the NIR wavelength range, the films are also highly reflective, which can help further reduce solar energy gain during summer, but may cause partial solar heating loss in winter.

aesthetical demands simultaneously and can serve as a flexible choice for both new buildings and the retrofitting of existing building envelopes. Moreover, the films are easy to clean and change, suggesting the potential practical value of our design, which could accelerate the switch towards sustainable building choices.

Results

Coloured low-emissivity film design. We designed the optical properties of the coloured low-emissivity films according to the solar spectrum and the thermal radiation spectrum. As illustrated in Fig. 1a, visible light (400–700 nm) and NIR (700 nm–2.5 μm) light account for around 45% and 49% of solar energy, respectively, and the thermal emission from room-temperature buildings and objects and the human body mainly falls into the wavelength range of 7–14 μm (MIR wavelength range). The design principle is to minimize radiative heat exchange between the indoor environment of buildings and the outdoor environment on the premise of visible colour appearance. The coloured low-emissivity film is thus engineered to be spectrally selective, as illustrated in Fig. 1b. In the visible light wavelength range, only light of the desired colour is reflected to fulfil the aesthetical function. In the MIR wavelength range, the films are highly reflective to minimize radiative thermal exchange with the environment. In summer, this reduces MIR radiative heat gain from hot surroundings; in winter, the decrease in MIR radiative heat loss to cold surroundings saves heating energy. In the NIR wavelength range, the films are designed to be highly reflective as well. This property can block NIR radiation from the sun to facilitate cooling energy savings in summer. In winter, the high NIR reflectance causes a partial loss of solar heat gain, but this loss can be minor because of the low solar irradiance, low sun angle and short daily sunlight time during winter, especially in cold climate areas[7]. For the trade-off between reducing MIR radiative heat loss and solar NIR heat gain in winter, we performed a detailed evaluation in the modelling section.

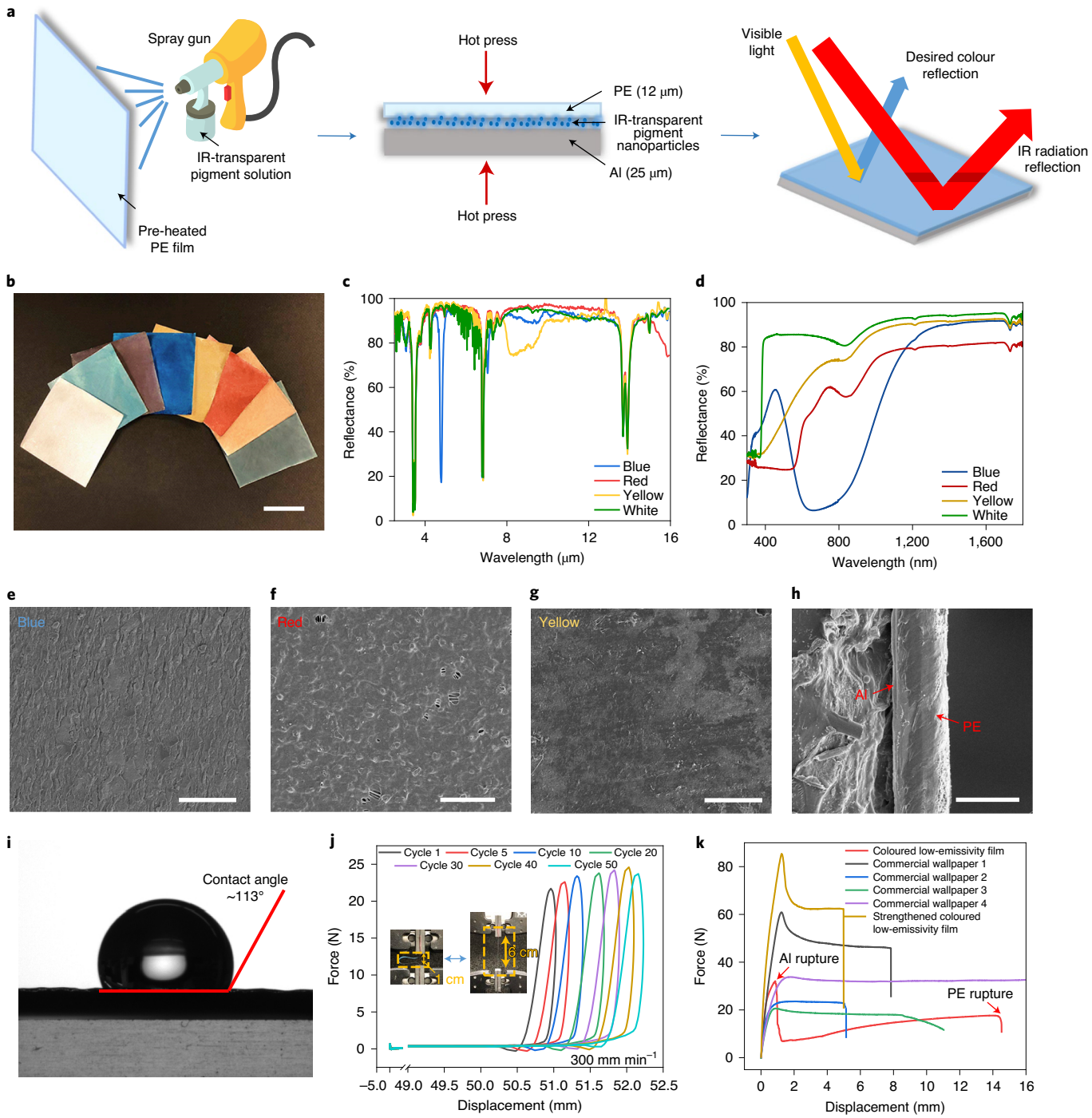

Fig. 2 | Fabrication and characterization of coloured low-emissivity films. a, Schematic illustration of the fabrication process for coloured low-emissivity films. **b**, Photograph of coloured low-emissivity films in various colours. Scale bar, 5 cm. **c**, Measured total reflectance spectra in the MIR wavelength range for white, blue, yellow and red samples. **d**, Measured total reflectance spectra of white, blue, yellow and red samples in the visible and NIR wavelength range. **e**–**g**, SEM images showing the surface morphology (PE side) of the blue (**e**), red (**f**) and yellow (**g**) low-emissivity films. Scale bars, 50 μm. **h**, SEM image of a cross section of the as-prepared coloured low-emissivity films. The PE layer partially encapsulates the Al edge. Scale bar, 50 μm. **i**, Water contact angle on the PE side. The contact angle is about 113°, showing decent hydrophobicity. **j**, Cyclic tensile test demonstrating the flexibility of coloured low-emissivity film. The inset photographs show the initial condition and final condition of the tested film strip in each cycle. **k**, Mechanical tensile test for the coloured low-emissivity film, commercial wallpapers and strengthened coloured low-emissivity film.

Fabrication and characterization. The fabrication process for coloured low-emissivity films is illustrated in Fig. 2a. We adopted the strategy of using a laminated bilayer to achieve the desired optical properties. The top layer is designed to selectively absorb visible wavelengths complementary to the desired colour while being highly transparent to infrared (IR) wavelengths. The bottom layer strongly reflects the transmitted IR light. Since the backscattered IR light is only weakly absorbed by the top layer, the two-layer structure exhibits high IR reflectance. Within the top layer, IR-transparent inorganic nanoparticles were incorporated as pigments: Prussian

blue, iron oxide (Fe_2O_3) and silicon (Si) nanoparticles for blue, red and yellow, respectively, which are the three primary colours[29,30], and zinc oxide (ZnO) nanoparticles for white. A spray-coating method was used to uniformly spray the IR-transparent pigments onto pre-heated polyethylene (PE) film that is also IR-transparent[31–33]. After the solvent evaporated, the pigment nanoparticles were uniformly loaded onto the PE substrate. The PE film together with IR-transparent pigments was then laminated with an Al layer during a hot-press process. The PE was melted at a high temperature to encapsulate the pigment nanoparticles, and the pigment–PE composite layer (top layer) was bonded to the Al layer (bottom layer). This completed the fabrication of the spectrally selective bilayer film.

The as-fabricated low-emissivity films in assorted colours are displayed in Fig. 2b. From left to right, the colours demonstrated are white, cyan, purple, blue, yellow, red, orange and dark grey. White, blue, yellow and red are the basic colours made by a single type of nanoparticles. Cyan, purple and orange were realized by mixing two of the three nanoparticles for the three primary colours (blue, yellow and red), whereas dark grey was made by mixing all three kinds of nanoparticles that yield the three primary colours. It is not difficult to enlarge the scale of manufacturing, since spray coating and roll-to-roll hot-press processes are mature in industry[34,35]. The total MIR reflectance was investigated with a Fourier transform infrared spectrometer equipped with a diffuse gold integrating sphere. Figure 2c shows the measured spectra of the films in three primary colours and white. They are all highly reflective for MIR light, showing about 90% reflectance (ρ) except for several narrow, sharp peaks. The IR transmittance is nearly 0 due to the IR-opaque Al; thus, the MIR emissivity is calculated to be ~0.1 (that is, $1-\rho$), which is ideal for low-emissivity materials (Supplementary Table 1). We measured the total reflectance of these low-emissivity films in the visible and NIR wavelength range as well. As shown in Fig. 2d, they all exhibit high reflectance (80–95%) for the NIR wavelengths. The spectra of films in the three primary colours reveal the different dominant reflection wavelengths around 450 nm, 600 nm and 750 nm, matching the visible colours of blue, yellow and red, respectively, while the white film shows relatively uniform reflectance of ~85% across the entire visible wavelength range. Compared with commercial paints, the high reflectance in NIR renders the coloured low-emissivity films capable of reflecting more solar energy than paint in the same colour. Due to the same reason, the yellow low-emissivity film even shows higher solar reflectance than commercial white paint (Supplementary Fig. 1). Through changing the concentrations of the pigments, the coloured low-emissivity films in various shades can be readily fabricated, and they still exhibit high reflectance in the MIR and NIR wavelength ranges and corresponding reflection peaks in the visible wavelength range (Supplementary Figs. 2–5). The spectra of low-emissivity films in purple, orange, cyan and dark grey are presented in Supplementary Fig. 6, exhibiting high IR reflectance.

Scanning electron microscope (SEM) images of the blue, red and yellow low-emissivity film surfaces (PE side) show that the pigment nanoparticles are well encapsulated by PE (Fig. 2e,g), which effectively enhances the colourfastness. The chemically inert PE serves as a decent protection layer. Figure 2h displays a cross-section SEM image of the bilayer film edge, verifying the good adhesion between the Al and PE. The PE layer also formed partial encapsulation on the Al edge, which provides extra adhesion stability. Moreover, we examined the contact angle of the top layer surface, which will be exposed in practical use. As presented in Fig. 2i, it appears hydrophobic, and the measured contact angle is around 113°, which renders it easy to clean and suitable for building application. The mechanical flexibility was inspected by a cyclic tensile test in which a blue low-emissivity film was pulled and bent at 300 mm min^{-1} for 50 cycles (inset of Fig. 2j). The sample strip remained intact

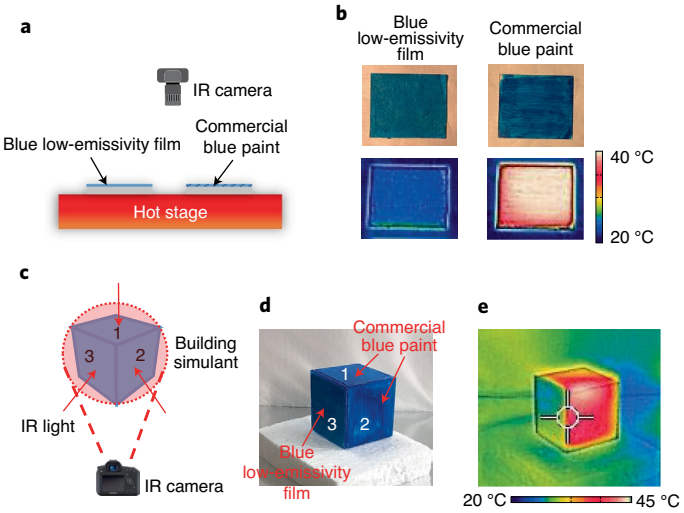

Fig. 3 | Visualized thermal effect of the coloured low-emissivity film. **a**, Schematic of the experiment examining the surface temperatures of samples on a hot stage. **b**, Optical photographs and thermal images of the blue low-emissivity film (left) and commercial blue paint (right) on the same hot stage. **c**, Schematic of the experiment observing the surface temperature of a building simulant covered by blue low-emissivity film and commercial blue paint under IR light. **d**, Optical photograph of the building simulant. Faces 1 and 2 were coated in commercial blue paint, while face 3 was covered by our blue low-emissivity film. **e**, Thermal image of the building simulant under IR light. The face covered by blue low-emissivity film shows a distinctly lower temperature.

after the 50-cycle test, and only negligible change was observed in the force-displacement curves (Fig. 2j). The mechanical flexibility makes the coloured low-emissivity films not only suitable for wall envelope surface installation but also appropriate extra layers for flexible window blinds (Supplementary Fig. 7). The tensile test result shows that the bilayer film can sustain a force of ~32 N before rupture (Fig. 2k), which is fair compared with commercial wallpaper. Moreover, our film can be further strengthened via adding a mechanically stronger back layer. As demonstrated in Fig. 2k, the strengthened sample can sustain even higher forces than the strongest commercial wallpaper we tested, and its surface optical properties are not affected (Supplementary Fig. 8). The environmental durability of the coloured low-emissivity film was also verified by a series of tests and was found to be satisfactory (see Methods, Supplementary Note 1 and Supplementary Figs. 9–12 for more information).

Thermal effect demonstration. The thermal effect resulting from the high IR reflectance of coloured low-emissivity films was visualized by a thermal camera. We selected the blue film as a representative sample and compared it with commercial blue paint. First, as illustrated in Fig. 3a, two identical plastic boards were placed on the same hot plate. One was covered by our blue low-emissivity film, while the other was coated in commercial blue paint. Their visible colours looked very similar (upper row, Fig. 3b), but the thermal images after temperature stabilization exhibited a notable difference (lower row, Fig. 3b). The board with commercial blue paint demonstrated very high emissivity (~1) (Supplementary Fig. 13). Hence, it was shown to have a high surface temperature under the thermal camera. In contrast, the blue low-emissivity film appeared much colder, revealing the diminished heat radiation. We also performed the experiment illustrated in Fig. 3c to observe the thermal effect under IR illumination. A cubic building simulant was made,

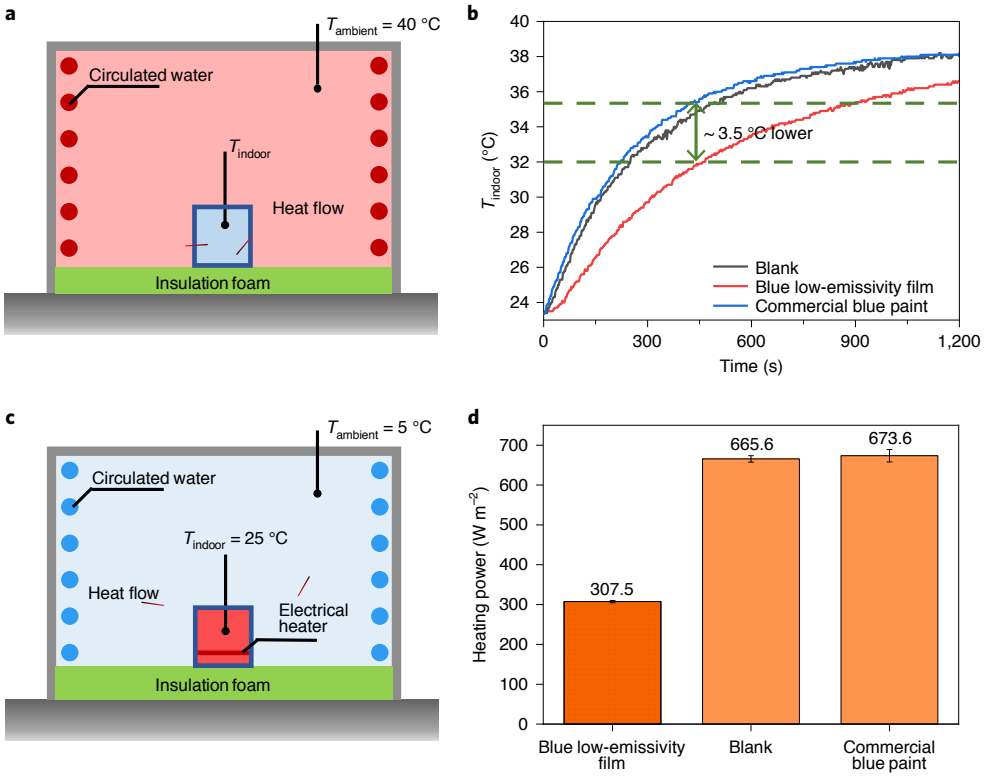

Fig. 4 | Thermal performance demonstration. a, Schematic illustration of the measurement apparatus for the heat gain test. A 40 °C ambient environment ($T_{ambient}$) was created by the circulated water system for the building simulant. Thermocouples were employed to measure the T_{indoor} curve of the building simulant. **b**, Measured indoor temperature curves of the building simulant with different surface modifications. The simulant with the blue low-emissivity film exhibited a slower temperature increase, verifying the reduced radiative heat gain. **c**, Schematic illustration of the measurement apparatus for the heat loss test. A 5 °C ambient environment was maintained by the circulated water system. An electric heater was inserted into the building simulant to generate heat and maintain the indoor temperature at 25 °C. **d**, Measured heating power of the electrical heater for the building simulant. The blue low-emissivity film greatly decreased the required heating power through reducing radiative heat loss. The error bars represent the standard deviation of the measured data.

and three of its faces (labelled as 1, 2 and 3) were illuminated by IR light. Faces 1 and 2 were coated with commercial blue paint, while face 3 was coated with blue low-emissivity film. The photograph in Fig. 3d demonstrates their comparable visible colours, showing that the blue low-emissivity film can well replace the conventional paint while maintaining aesthetical function. Nevertheless, because our film substantially reflects the incoming IR light, extremely distinct surface temperatures were observed in the thermal image of the building simulant with two types of surface coatings (Fig. 3e). This test showed that coloured low-emissivity film can efficiently prevent overheating by rejecting the incident thermal radiation.

To further investigate the thermal performance of the coloured low-emissivity films, we tested building simulants in artificial hot and cold environments. We used an enclosed chamber equipped with circulated water to create hot or cold circumstances. In these experiments, building simulants covered by blue low-emissivity film, commercial blue paint or no covering (blank) were measured in parallel (Supplementary Fig. 14). Thermocouples were fixed at identical positions in each building simulant to measure the inside temperature (denoted as T_{indoor}). As diagrammed in Fig. 4a, we studied the indoor heat prevention performance in a 40 °C environment. The building simulant was first stabilized at room temperature (~23.5 °C) and then transferred into the 40 °C environment with interior temperature recording on. No extra cooling source was included in the building simulant, so all the building simulants would ultimately reach thermal equilibrium at the same temperature as the hot environment. Nevertheless, their temperature increase curves are valuable for comparing their ability to resist being heated. The heat capacity change and thermal conductance change caused by coating the simulants with the blue low-emissivity film or the blue paint can be considered negligible, since the coatings were very thin. The building simulant with the blue low-emissivity film clearly showed a delay in temperature increase, in contrast to the simulant with blue paint and the blank simulant. T_{indoor} was lower for the simulant with the blue low-emissivity film at all times before the equilibrium was reached (Fig. 4b). At 500 s, for example, the measured T_{indoor} was approximately 3.5 °C lower than that for other two. The measured interior wall and exterior wall temperature curves are presented in Supplementary Fig. 15; these exhibited similar trends. These results verify that the high IR reflectance of the blue low-emissivity film efficiently diminished heat gain from the environment. We also conducted measurements for the building simulants in a cold environment (5 °C) mimicking winter conditions (Fig. 4c). In this experiment, an electric heater was added to each building simulant to provide constant heating power that was adjusted to maintain a constant T_{indoor} at 25 °C. As expected, the building simulant with our blue low-emissivity film required a heating power of only ~307.5 W m^{-2}, while the other two needed about 670 W m^{-2}, which is more than twice the power required for the blue low-emissivity film (Fig. 4d). This result proves that the coloured low-emissivity films are capable of greatly reducing indoor heat loss to the cold environment, thus saving heating energy.

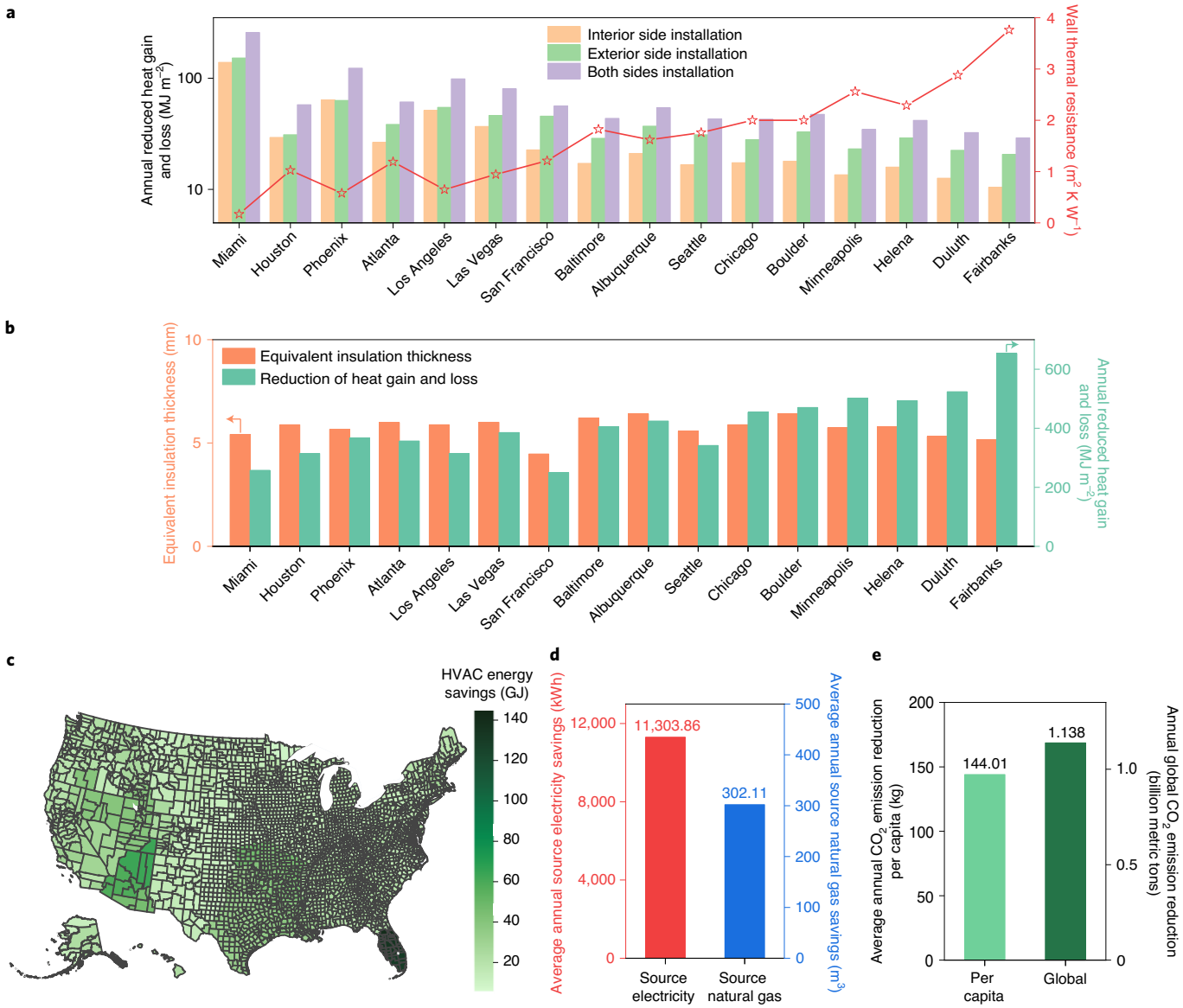

Fig. 5 | Modelled annual reduction of heat transmission and evaluation of building energy savings. a, Calculated annual reduction of heat gain and loss per installation wall area for installation on wall interior surface, exterior surface and both sides for 16 representative cities in various climate zones. **b**, Calculated equivalent insulation thickness for double-sided installation of coloured low-emissivity materials on non-insulated walls and its annual reduction of heat gain and loss per installation wall area. **c**, HVAC energy-savings map across the United States with coloured low-emissivity film installation on walls for a typical midrise apartment building. **d**, Predicted average annual source electricity and source natural gas savings for the modelled building. **e**, Predicted average annual CO_2 emission reduction per capita and globally.

Thermal modelling and energy-saving evaluation. We developed a thermal model (see Supplementary Note 2, Supplementary Figs. 16–20 and Supplementary Table 2 for more details) to quantify the reduction of heat gain and loss through a wall by applying coloured low-emissivity films[36]. We considered a post-1980 midrise apartment building's exterior walls, defined by the US Department of Energy, as the study object, and we calculated an average effect of heat transmission reduction per installation wall area. This model is used to estimate the heat transmission reduction through a wall by changing its surface optical properties with some simplification, including a steady-state assumption and neglect of possible solar gain from interior wall surfaces, complicated inner structure and furnishings inside the building. The annual total reduction of heat gain or loss per unit of exterior wall area was calculated for film installation on the wall's interior surface, exterior surface and double-sided surfaces in 16 representative cities in different climate zones with differing original wall insulation conditions (Fig. 5a). For all locations, we clearly demonstrated the feasibility of heat transmission reduction through the wall by installation of our materials. Our coloured low-emissivity films can bring about a reduction of heat gain or loss from dozens to hundreds of MJ per installation wall area. This effect is especially strong for cities in the southern and middle United States. Specifically, taking Miami as an example, the double-sided installation can achieve heat transmission reduction of 257.6 MJ m^{-2}. We also extracted the average radiative and convective energy transfer component with and without the film installation (Supplementary Fig. 21). The differences in these components clearly show that the radiative energy transfer (either

gain or loss) can be obviously reduced. In addition, to analyse the influence of the surroundings' shading, we calculated the reduction of heat gain and loss for Miami and Fairbanks with varied urban densities in addition to the isolated condition (see Supplementary Note 3 and Supplementary Figs. 18 and 22 for more information).

The above calculation is based on existing walls with different thermal resistances. To further assess the heat transmission reduction effect, we calculated for 16 cities the equivalent insulation layer thickness that would achieve the same reduction of heat gain or loss as our low-emissivity films, assuming the films are installed on both sides of non-insulated wall surfaces, as explained in Supplementary Fig. 23. The green columns in Fig. 5b exhibit the annual reduction of heat gain and loss per unit wall area, and the orange columns show that the double-sided installation of extremely thin coloured low-emissivity films (~40 μm for a single one) on non-insulated walls is equivalent to adding around 6 mm of insulation material ($0.049\ W\ m^{-1}\ K^{-1}$), which is more than 70 times as thick as our films. This high equivalent insulation layer thickness indicates that coloured low-emissivity films can not only benefit heat insulation of existing buildings with varied wall thermal resistance but also decrease insulation thickness and provide design flexibility for new buildings.

We then used EnergyPlus to evaluate HVAC energy-saving performance (see Methods for more details). We adopted the reference building models (post-1980 midrise apartment) in EnergyPlus defined by the US Department of Energy. Whereas our customized thermal model focuses on the heat transmission reduction of a wall, EnergyPlus comprehensively considers the heat exchange of the whole building coupled with complicated HVAC systems and outputs the final HVAC energy use of the building. The HVAC energy use (cooling, heating, fans and water systems) was calculated for the building with conventional wall materials and with walls that have the surface properties of our coloured low-emissivity material. The energy use difference was exactly the HVAC energy savings. The baseline energy use for cooling, heating, fans and the whole HVAC system in 16 selected cities is displayed in Supplementary Fig. 24a. When our coloured low-emissivity materials were applied to walls, energy savings for cooling, heating, and fans were observed in each city. As shown in Supplementary Fig. 24b,c, up to 77.02 GJ of cooling energy (corresponding to 9.88% of baseline cooling energy), 17.53 GJ of heating energy (13.17% of baseline heating energy) and 29.91 GJ of fan energy (16.43% of baseline fan energy) can be saved for such a typical midrise apartment building. In total, up to 124.46 GJ can be saved, which equals 11.37% of baseline energy use for cooling, heating and fans. If we consider the whole HVAC system including water systems, the HVAC energy-saving ratio is still as high as 9.87%. Moreover, we evaluated the annual HVAC energy savings brought about by coloured low-emissivity film installation for such a prototype midrise apartment across the United States using EnergyPlus; the resulting energy-savings map is shown in Fig. 5c.

We also converted the energy savings of this modelled building into annual source electricity savings and source natural gas savings. On the basis of our calculation using EnergyPlus, an average of 11,303.86 kWh of source electricity and 302.11 m^3 of source natural gas can be saved for such a building (Fig. 5d), which equals approximately 8,568.8 kg CO_2 emission reduction for the whole building and 144.01 kg per capita. The roughly estimated total annual global CO_2 emission reduction is 1.14 billion metric tons (Fig. 5e) based on the world population (https://worldpopulationreview.com/). This estimate equals roughly a 3% reduction considering the approximately 36.4 billion metric tons of global CO_2 emissions per year (https://ourworldindata.org/co2-emissions).

Discussion

Aiming to provide a new material choice for energy-efficient buildings and environmental sustainability, we developed a category of coloured low-emissivity films, which demonstrate thermal function and aesthetical appeal simultaneously. In addition to the selective reflection of the desired visible colour, the high IR reflectance of ~90% enables effective reduction of radiative heat exchange with the ambient surroundings in both warm and cold weather, saving both heating and cooling energy with a single material.

However, a greater energy-saving effect can be achieved if the film can show adaptive high NIR absorptance during winter to make the most of solar heating. Moreover, we expect that an anisotropic MIR property that is highly emissive to the sky while highly reflective to the ambient surroundings will further benefit cooling energy savings in summer, even if the view factor to the sky is much smaller than that to the surroundings for building walls.

Our simulation verifies the effect of heat transmission reduction through walls and evaluates the energy-saving performance by the installation of our films. The amount of heat transmission reduction and HVAC energy savings depends on the weather environment and the original thermal insulation conditions of the wall; thus, the values vary for the simulated building in different cities. Overall, a negative correlation between the heat transmission reduction (and energy savings) and the original wall thermal insulation was observed in our simulation, because the effect of radiative heat transfer reduction is weakened when the wall thermal insulation is originally very good. The environmental conditions also play an important role, which cannot be ignored. These factors should be taken into account in practical applications.

With proper hydrophobicity, decent mechanical properties and weather durability, these films provide a flexible solution for both existing and new buildings to minimizing radiative heat exchange between the indoor environment and the outdoor surroundings to achieve all-year energy savings, while satisfying the necessary aesthetical demand. We believe that the coloured low-emissivity films are promising for energy-efficient building applications and can make a positive contribution to global carbon neutrality and sustainability.

Methods

Fabrication of coloured low-emissivity films. The selected pigment nanoparticles (Prussian blue (ACROS Organics), Fe_2O_3 (Sigma-Aldrich, 99%), Si (Sigma-Aldrich, < 100 nm, ≥ 98% trace metals basis) and ZnO (Sigma-Aldrich, 99.9%)) for the corresponding colours (a single type of nanoparticles or mixed) were dispersed in ethyl alcohol (denatured, Fisher Scientific) with the assistance of magnetic stirring and sonication. Nanoporous PE films (Teklon, 12 μm, Entek International LLC) were fixed on a vertical hot plate as the spraying substrate. The nanoparticle solutions were loaded into a spray gun (Yattich, YT-191) and sprayed onto the pre-heated PE films. By adjusting the spray speed and spray times, the desired mass loading of pigments could be achieved after the evaporation of ethyl alcohol. The mass of the PE films was measured before spray coating so that the loaded pigment mass could be calculated by weighing the PE films after the spray-coating process. Next, the PE films with pigments were hot pressed with Al foil (25 μm, Reynolds) using a hot press machine (MTI).

Material characterization. The MIR reflectance was measured by a Fourier transform infrared spectrometer (Model 6700, Thermo Scientific) accompanied with a diffuse gold integrating sphere (PIKE Technologies). The visible and NIR reflectance was measured by UV-Vis-NIR spectrometers (Agilent, Cary 6000i and Jasco V-670) equipped with diffuse reflectance accessories. SEM images were taken with an FEI Nova NanoSEM (5 kV). The contact angle was measured by a contact angle goniometer (Rame-Hart 290). The sample mass was measured by an analytical balance (Ohaus Pioneer, 0.0001 g readability).

Mechanical test. The cyclic tensile test and tensile strength test were measured by an Instron 5565. For the cyclic test, the sample was 2 cm wide and 8 cm long, and the gauge distance was 1 cm at the beginning and became 6 cm at the end of every cycle. The displacement rate was $300\ mm\ min^{-1}$. The cyclic test was performed for 50 cycles. For the tensile strength test, the sample was 2 cm wide and 4 cm long, and the gauge distance was 2 cm long. The displacement rate was $10\ mm\ min^{-1}$.

Thermal measurements. All the thermal images were taken with a thermal camera (FLIR, E6). For the thermal images on a hot plate, two identical acrylic boards (1.5 mm thick, McMaster-Carr) were covered with blue low-emissivity film and commercial blue paint (The One, gloss blue), respectively, and placed on a 40 °C

hot plate. For the thermal images of the building simulant under IR light, an IR light bulb illuminated a cubic building simulant made with acrylic boards (2.5 cm side length). Blue low-emissivity film and commercial blue paint were applied on different faces. For the thermal measurements in the temperature-regulated chamber, cubic building simulants with 5 cm side length were assembled with acrylic boards (1.5 mm thick, McMaster-Carr). Small holes (1 mm in diameter) were cut with a CO_2 laser cutter (Epilog Fusion M2) for inserting thermocouples (K type, Omega Engineering) into the building simulants. A data logger (HH374, Omega Engineering) was used to record the temperature data of the building simulants. The air temperature in the enclosed chamber was measured by a thermocouple (K type, Omega Engineering) as well, and it was controlled by a circulated water system. A polyimide insulated flexible heater (McMaster-Carr, ~25 cm^2) connected to a power supply (Keithley 2400) was fixed in the building simulants to provide heating power in the 5 °C ambient tests. The supplied power density was adjusted for different samples to make the indoor temperature of the building simulants stable at 25 °C. For the building simulants with different samples, we fixed the positions of the thermocouples and heaters and the location in the testing chamber during measurements to make the measurements as parallel as possible to provide reasonable comparison.

Environmental durability tests. For the high-temperature test, the sample was put into an oven (MTI, SS-00AB table dry oven) at a constant temperature of 60 °C and maintained for one week. For the low-temperature test, the sample was put in a foam insulation box filled with liquid nitrogen for two hours. The tested sample was soaked in liquid nitrogen during the whole testing process. For the acid test, concentrated sulfuric acid (95–98%, Sigma-Aldrich) was diluted with deionized water. Its pH was adjusted to be around 4 (tested by pH test strips, EMD Millipore). The sample was immersed in the solution continuously for one week. For the alkali test, potassium hydroxide solution (pH = 10, tested by pH test strips, EMD Millipore) was prepared with potassium hydroxide (Sigma-Aldrich) and deionized water. The sample was immersed in the solution continuously for one week. For the water flushing test, the test method was modified from ASTM D7377. The sample was fixed with a tilt angle of ~45° at a distance of 5 cm from the water faucet. The flow rate of water from the faucet was ~300 ml min^{-1}. Water hit the sample and then flowed into the sink. For the UV exposure test, the test method was modified from ASTM D4587. The sample was illuminated by a UV lamp (72 W) directly for one week. The distance between the sample and the lamp was ~7 cm. The apparatus was enclosed in an opaque chamber. For the wind test, the sample was fixed onto a glass plate with the coloured side facing up. An adjacent electric fan was turned on, providing wind for the sample with a speed of around 1.5 m s^{-1} (HoldPeak 866B Digital Anemometer). For the abrasion test, the sample piece was attached to a glass slide, which was placed on sandpaper (Fandeli, grit size 400) facing down. A 100 g weight was placed on the top side of the glass. The glass was moved 10 cm along a ruler (point A to B), 10 cm perpendicular to the ruler (point B to C), 10 cm parallel to the ruler (point C to D) and 10 cm perpendicular to the ruler to the origin point (point D to A). The above process was defined as one cycle (Supplementary Fig. 12a). The visual appearance, surface morphology, mass and spectra were examined after the tests to evaluate the durability of the sample.

Energy-saving calculation by EnergyPlus. We used a commercial reference building model (post-1980 midrise apartment) defined by the US Department of Energy in EnergyPlus version 9.5[37]. The model building has four stories, including 31 apartments plus an office. The building shape is rectangular with an aspect ratio of 2.74 (length, 46.33 m; width, 16.91 m; height, 12.19 m). The building's north axis is 0 degrees to true north. The total floor area is 3,135 m^2. The windows cover 15% of the total wall surface area. Supplementary Fig. 16 shows a sketch of the building. The internal gains and HVAC system have been comprehensively designed in the models. Split HVAC system units are in each apartment and the office (DX cooling and gas furnace). The indoor air temperature set-point was set constantly as 22 °C, and the external weather utilized hourly weather data for a typical meteorological year (TMY3). The HVAC energy use was calculated for the baseline building models with conventional wall properties (as set in the downloaded EnergyPlus models) and building models with modified wall surface optical properties by applying our material (the values were determined by experimentally measured data). Comparing the energy consumption between them, we obtained the all-year energy savings for cooling, heating, fans and total HVAC. To analyse the energy-saving performance in regions across different climate zones, we present 16 representative cities in 16 climate zones in the United States (Miami, Houston, Phoenix, Atlanta, Los Angeles, Las Vegas, San Francisco, Baltimore, Albuquerque, Seattle, Chicago, Boulder, Minneapolis, Helena, Duluth and Fairbanks). The energy-savings map was plotted on the basis of EnergyPlus calculations for over 100 cities across the United States. The source electricity savings and source natural gas savings were also calculated by EnergyPlus using the site-to-source conversion factors. For natural gas, a conversion factor of 25.866 m^3 GJ^{-1} was adopted to calculate the natural gas volume savings (https://www.eia.gov/energyexplained/units-and-calculators/energy-conversion-calculators.php). CO_2 emission reduction was calculated by converting the electricity savings and natural gas savings using the relevant factors: 1 kWh electricity = 0.709 kg CO_2 and 1 m^3 natural gas = 1.935 kg CO_2 (https://www.epa.gov/energy/greenhouse-gas-equivalencies-calculator).

Data availability

The original data that support the findings of this study are available from the corresponding author upon request.

Code availability

The code for the building energy consumption model can be made available upon request.

Received: 3 May 2021; Accepted: 9 November 2021;
Published online: 23 December 2021

References

1. Yin, X., Yang, R., Tan, G. & Fan, S. Terrestrial radiative cooling: using the cold universe as a renewable and sustainable energy source. *Science* **370**, 786–791 (2020).
2. *Quadrennial Technology Review: An Assessment of Energy Technologies and Research Opportunities* Ch. 5 (US Department of Energy, 2015); https://www.energy.gov/sites/prod/files/2017/03/f34/qtr-2015-chapter5.pdf
3. *Heating and Cooling* (US Department of Energy, accessed 16 April 2021); www.energy.gov/heating-cooling
4. Li, T. et al. A radiative cooling structural material. *Science* **364**, 760–763 (2019).
5. Goetzler, W. *Energy Savings Potential and RD&D Opportunities for Commercial Building HVAC Systems* (US Department of Energy, 2017).
6. Jelle, B. P. Traditional, state-of-the-art and future thermal building insulation materials and solutions—properties, requirements and possibilities. *Energy Build.* **43**, 2549–2563 (2011).
7. Pisello, A. L. State of the art on the development of cool coatings for buildings and cities. *Sol. Energy* **144**, 660–680 (2017).
8. Zhai, Y. et al. Scalable-manufactured randomized glass–polymer hybrid metamaterial for daytime radiative cooling. *Science* **355**, 1062–1066 (2017).
9. Mandal, J. et al. Hierarchically porous polymer coatings for highly efficient passive daytime radiative cooling. *Science* **362**, 315–319 (2018).
10. Chen, Y. et al. Colored and paintable bilayer coatings with high solar-infrared reflectance for efficient cooling. *Sci. Adv.* **6**, eaaz5413 (2020).
11. Zhou, L. et al. A polydimethylsiloxane-coated metal structure for all-day radiative cooling. *Nat. Sustain.* **2**, 718–724 (2019).
12. Raman, A. P., Anoma, M. A., Zhu, L., Rephaeli, E. & Fan, S. Passive radiative cooling below ambient air temperature under direct sunlight. *Nature* **515**, 540–544 (2014).
13. Hernández-Pérez, I. et al. Thermal performance of reflective materials applied to exterior building components—a review. *Energy Build.* **80**, 81–105 (2014).
14. Li, X. et al. Integration of daytime radiative cooling and solar heating for year-round energy saving in buildings. *Nat. Commun.* **11**, 6101 (2020).
15. Martilli, A., Clappier, A. & Rotach, M. W. An urban surface exchange parameterisation for mesoscale models. *Bound. Layer Meteorol.* **104**, 261–304 (2002).
16. Albatici, R., Passerini, F., Tonelli, A. M. & Gialanella, S. Assessment of the thermal emissivity value of building materials using an infrared thermovision technique emissometer. *Energy Build.* **66**, 33–40 (2013).
17. Avdelidis, N. P. & Moropoulou, A. Emissivity considerations in building thermography. *Energy Build.* **35**, 663–667 (2003).
18. Aditya, L. et al. A review on insulation materials for energy conservation in buildings. *Renew. Sustain. Energy Rev.* **73**, 1352–1365 (2017).
19. Jelle, B. P., Kalnæs, S. E. & Gao, T. Low-emissivity materials for building applications: a state-of-the-art review and future research perspectives. *Energy Build.* **96**, 329–356 (2015).
20. Guo, W., Qiao, X., Huang, Y., Fang, M. & Han, X. Study on energy saving effect of heat-reflective insulation coating on envelopes in the hot summer and cold winter zone. *Energy Build.* **50**, 196–203 (2012).
21. Juanicó, L. E. Thermal insulation of roofs by using multiple air gaps separated by insulating layers of low infrared emissivity. *Constr. Build. Mater.* **230**, 116931 (2020).
22. Tenpierik, M. J. & Hasselaar, E. Reflective multi-foil insulations for buildings: a review. *Energy Build.* **56**, 233–243 (2013).
23. Medina, M. A. A comprehensive review of radiant barrier research including laboratory and field experiments. *ASHRAE Trans.* **118**, 400–407 (2012).
24. Principi, P. & Fioretti, R. Thermal analysis of the application of PCM and low emissivity coating in hollow bricks. *Energy Build.* **51**, 131–142 (2012).
25. Fantucci, S. & Serra, V. Experimental assessment of the effects of low-emissivity paints as interior radiation control coatings. *Appl. Sci.* **10**, 842 (2020).

26. Joudi, A., Svedung, H., Cehlin, M. & Rönnelid, M. Reflective coatings for interior and exterior of buildings and improving thermal performance. *Appl. Energy* **103**, 562–570 (2013).
27. Fantucci, S. & Serra, V. Low-E paints enhanced building components: performance, limits and research perspectives. *Energy Procedia* **126**, 274–281 (2017).
28. Shen, H., Tan, H. & Tzempelikos, A. The effect of reflective coatings on building surface temperatures, indoor environment and energy consumption—an experimental study. *Energy Build.* **43**, 573–580 (2011).
29. Cai, L. et al. Temperature regulation in colored infrared-transparent polyethylene textiles. *Joule* **3**, 1478–1486 (2019).
30. Peng, Y. & Cui, Y. Advanced textiles for personal thermal management and energy. *Joule* **4**, 724–742 (2020).
31. Hsu, P.-C. et al. Radiative human body cooling by nanoporous polyethylene textile. *Science* **353**, 1019–1023 (2016).
32. Peng, Y. et al. Nanoporous polyethylene microfibres for large-scale radiative cooling fabric. *Nat. Sustain.* **1**, 105–112 (2018).
33. Hsu, P.-C. et al. A dual-mode textile for human body radiative heating and cooling. *Sci. Adv.* **3**, e1700895 (2017).
34. Reale, A. et al. Spray coating for polymer solar cells: an up-to-date overview. *Energy Technol.* **3**, 385–406 (2015).
35. Chen, Y. et al. Roll-to-roll production of metal–organic framework coatings for particulate matter removal. *Adv. Mater.* **29**, 4–9 (2017).
36. Fan, L., Li, W., Jin, W., Orenstein, M. & Fan, S. Maximal nighttime electrical power generation via optimal radiative cooling. *Opt. Express* **28**, 25460–25470 (2020).
37. Crawley, D. B., Pedersen, C. O., Lawrie, L. K. & Winkelmann, F. C. EnergyPlus: energy simulation program. *ASHRAE J.* **42**, 49–56 (2000).

Acknowledgements

We thank Q. Li for helpful discussion and kind help. Part of this work was performed at the Stanford Nano Shared Facilities and the Stanford Nanofabrication Facility. S.F. acknowledges the support of the US Department of Energy (grant no. DE-FG-07ER46426).

Author contributions

Y.C. and Y.P. conceived the idea. Y.P. designed the experiments and performed the material preparation and characterization with the help of Y.Y., Z.H., Y.M., J.T. and J.Z. L.F. and W.J. performed the modelling work. S.Z. and X.L. provided helpful discussion on EnergyPlus. L.C.G. helped with writing the manuscript. Y.C., A.M. and S.F. supervised the project. All the authors provided discussion and comments.

Competing interests

The authors declare no competing interests.

Additional information

Supplementary information The online version contains supplementary material available at https://doi.org/10.1038/s41893-021-00836-x.

Correspondence and requests for materials should be addressed to Yi Cui.

Peer review information *Nature Sustainability* thanks Tao Ma and the other, anonymous, reviewer(s) for their contribution to the peer review of this work.

Reprints and permissions information is available at www.nature.com/reprints.

Publisher's note Springer Nature remains neutral with regard to jurisdictional claims in published maps and institutional affiliations.